Prediction of Noise from Turbulent Boundary Layers with Suction

Achyuth Rajendran* and Steven A. E. Miller†
University of Florida, Gainesville, Florida, 32611

Suction is used to control boundary layers on wings, inlets, wind tunnels, and other aerospace devices. Designing suction mechanisms to minimize noise generation is critical to reduce aeroacoustic loading and to conduct low-noise measurements. A semi-empirical acoustic analogy is used to predict the noise from the boundary layer when suction is present. The model depends on local turbulent boundary layer statistics. These statistics are calculated via a steady Reynolds-averaged Navier-Stokes computational fluid dynamics solver. Acoustic predictions are conducted at three subsonic Mach numbers over a flat plate without a pressure gradient. To study the effect of suction, a single thin port is placed at the wall with constant back pressure. At each Mach number, the change of sound pressure level with frequency is compared to a corresponding case with no suction. We observe that the presence of suction leads to increased noise at low Mach numbers and decreased noise at higher Mach numbers.

Nomenclature

Symbols	Description
D	Suction port diameter
F_t	Far-field term
f	Frequency
$\overline{u_c}$	Local convection velocity
TKE	Turbulent kinetic energy
l_{sy}	Turbulent length scale in the cross-stream direction
l_{sz}	Turbulent length scale in the span-wise direction
A_{ijlm}	Coefficient matrix
S	Auto-power spectral density
T	Temperature
u	Fluid velocity in the streamwise direction
X	Observer position
u_τ	Wall friction velocity
U^+	Velocity coordinate (uu_τ^{-1})
Y^+	Wall coordinate ($u_\tau y \nu^{-1}$)
Greek Symbols	
δ	Boundary layer thickness
η	Vector from origin to a point within the turbulent boundary layer
ξ	Vector between sources
ρ	Density
ν	Kinematic viscosity
ω	Turbulence dissipation energy
Non-Dimensional Numbers	
M_∞	Free-stream Mach number
Re	Reynolds number
Re_θ	Momentum thickness Reynolds number
St	Strouhal number

Introduction

Suction as a form of boundary layer control is a well-known mechanism used on wings, inlets, wind tunnel test sections and other aerospace devices. There are several methods in existence to artificially control the behaviour of the boundary layer. Prandtl [1], as early as 1904, described several experiments in which the boundary layer was controlled. One of his earliest works dealt with applying suction in the wake of a rotating cylinder to demonstrate the effect of suction in reattaching flows. Suction is one of many forms of boundary layer control. Other active and passive forms include motion of the solid wall, acceleration of the boundary layer (blowing), injection of a different gas (binary boundary layers), prevention of transition to turbulent flows by the provision of suitable shapes (laminar aerofoils), or cooling of the wall. A detailed description of these methods can be found in Schlichting [2].

Suction in turbulent boundary layers has been thoroughly studied both experimentally and numerically over the years. The process of interfering with the structure of a turbulent boundary layer in order to obtain a desirable effect, such as for reduction of the frictional drag or delay in flow separation, has been the subject of numerous studies.

Oyewola et al. [3] experimentally examined the effect of concentrated wall suction through a porous strip on a turbulent boundary layer and found that the skin friction coefficient, c_f, is strongly modulated by the momentum

*M.S. Student, Mechanical and Aerospace Engineering, PO BOX 116250, Gainesville, FL, 32611, and AIAA Student Member, arajendran1@ufl.edu.

†Assistant Professor, Mechanical and Aerospace Engineering, PO BOX 116250, Gainesville, FL, 32611, and AIAA Senior / Lifetime Member. saem@ufl.edu / saemiller@gmail.com

thickness Reynolds number, Re_θ. They also proposed that if pseudo-relaminarisation were to be obtained, then the ratio of Re_θ and suction rate must not exceed a particular critical value. Zhu and Antonia [4] examined the effect of suction applied through a porous strip on the structure of a low Reynolds number turbulent boundary layer and observed that the Reynolds shear stress was significantly reduced in the vicinity of the suction strip, and it recovers further downstream, attaining no suction value. Djenidi et al. [5], through Laser Doppler Velocimetry (LDV) and Planar Laser Induced Fluorescence (PLIF), reported that pseudo-relaminarisation occurred behind the suction strip when the suction rate is relatively high. Also, three-dimensional features of the near-wall structures were reduced due to suction. Reynolds and Saric [6] showed experimentally that suction, applied through discrete porous strips, can be as effective as suction applied continuously over a much longer stream-wise length.

There have been a number of numerical investigations in this area as well. For example, Antonia et al. [7] performed direct numerical simulation (DNS) for a zero pressure gradient turbulent boundary layer at moderate Re and found there was a significant increase in anisotropy in the near-wall region when suction is applied uniformly at the wall. Park and Choi [8] performed DNS on a turbulent boundary layer for a span-wise slot. They observed that for both blowing and suction, the stream-wise turbulent intensity recovers quickly, while other components of the turbulent intensities and Reynolds shear stress recover over a longer distance. Kametani et al. [9] performed large-eddy simulation (LES) of a spatially evolving turbulent boundary layer with uniform suction and blowing at moderate Re, and they were able to obtain more than 10% drag reduction and enhancement. Bobke et al. [10] simulated turbulent asymptotic suction boundary layers with LES, and they observed that components of the Reynolds stress tensors were overall reduced, but exhibit a logarithmic increase with decreasing suction rates.

Present Approach

Generally, previous research examined the effect suction has on turbulent structures and wall statistics, and suction is presently used to control boundary layers on aerospace vehicles. However, no studies have been performed to study the acoustic radiation from turbulent boundary layers in the presence of suction. This paper presents the first such study to the authors' knowledge. This is important as aerospace structures such as wings have suction as a form of flow control within them and designing wings with low aerodynamic noise is important for communities near airports. To isolate the effect of suction on the boundary layer and its associated noise, we conduct simplified numerical simulations of flat plate turbulent boundary layers with and without suction ports. These numerical simulations are then used with an acoustic analogy approach, which was previously developed and validated to predict the radiated noise. Predictions of spectral density of acoustic pressure are conducted using the approach of Miller [11]. Flow variables in the cross-stream direction relative to the flow direction at a particular point on the plate after suction are used to generate the acoustic spectra observed.

Mathematical Model

A. Aerodynamics of the Turbulent Boundary Layer

We model the flow with the steady Reynolds-averaged Navier-Stokes (RANS) equations closed by the Menter k-ω shear stress transport (SST) turbulence model [12]. Two computational domains are created with corresponding computational grids. The first is for a flat plate, and the second is the same flat plate with a suction port. The grids are created with Gmsh [13]. Figure 1(a) shows the computational domain without the suction port, and Fig. 1(b) shows the computational domain with the suction port. Here, the suction port resides at a distance of 0.99 m from the leading edge. The port spans 0.02 m across with a depth of 0.25 m. The leading edge of the plate is at the origin. Flow enters the domain from the left at an inlet boundary condition. The flow Mach number depends on the specification of the Mach number and atmospheric pressure (101.325 kPa). It exits the right side of the domain at an outlet boundary condition, which enforces the zero-pressure-gradient condition. A free-stream boundary condition is set at the top. An Eulerian slip wall resides before the plate ($x < 0$). A no-slip adiabatic wall represents the plate surface. The no-slip condition applies to the walls of the suction port as well. At the bottom of the suction port, a second static pressure outlet of 100 kPa is used to exhaust the flow.

B. Aeroacoustics of the Turbulent Boundary Layer

The cross-spectral acoustic analogy of Miller [11] is used to predict the statistics of acoustic pressure. This approach is a generalization of the acoustic analogy of Lighthill [14]. We retain the far-field term only, as it was previously shown

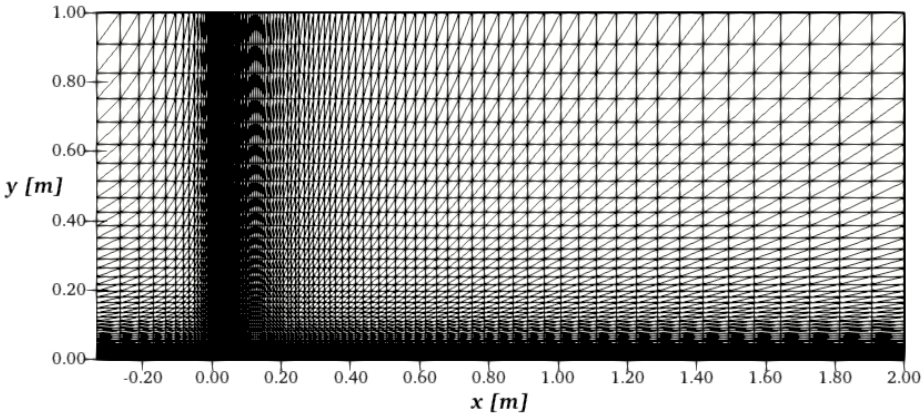

(a)

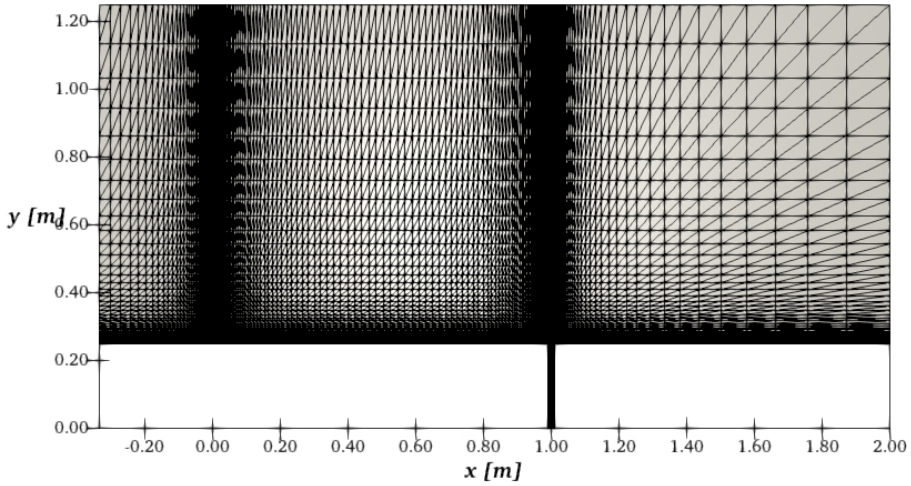

(b)

Fig. 1 Computational domain a) without and b) with the suction port.

that the mid-field and near-field terms contribute very little acoustic energy from a subsonic turbulent boundary layer. It was shown that the spectral density of the acoustic pressure from a turbulent boundary layer with one particular form for the two-point cross-correlation of the equivalent source is

$$S(X,\omega) = \frac{1}{4\pi^2} \int_{-\infty}^{\infty} \int_{-\infty}^{\infty} \int_{-\infty}^{\infty} \int_{-\infty}^{\infty} A_{ijlm} l_{sy} l_{sz} F_t \mathcal{I} \, d\xi d\boldsymbol{\eta}, \tag{1}$$

where A_{ijlm} is a coefficient matrix, $\boldsymbol{\xi}$ is a vector between two sources in the axial direction, and $\boldsymbol{\eta}$ is a vector from the origin to a point within the turbulent boundary layer. F_t is the far-field term. We approximate A_{ijlm} as $A_{ijlm} \approx \overline{\rho}\,\overline{\rho}'\overline{u_i u_j u'_l u'_m}$. A Gaussian based decay model of the two-point cross-correlations of the equivalent source is used to perform the integrations. Within Eqn. 1, $\mathcal{I}$ is shown in Miller [11], and is the result of analytical integration of the two-point cross-correlation model. We use the approach of Efimtsov [15] to estimate the length scales of the flow, which are l_{sy} and l_{sz}. The subscripts y and z indicate the cross-stream and span-wise flow directions, respectively. The

length scales are dependent on the local convection velocity, which is estimated as $\overline{u_c} = 0.70\,\overline{u}$. ξ and η denote the streamwise and cross-stream directions. Equation 1 is evaluated by approximating the integrals in these directions. Following the approach of Powell [16], a mirror source is used to account for reflection of acoustic waves at the wall. Integration is performed using the boundary layer profile derived from the steady RANS solution. The sound pressure level (SPL) spectra is then calculated for each frequency by

$$\mathrm{SPL_f} = 20\log_{10}\frac{S^{1/2}(X,\omega)}{2\times10^{-5}\ \mathrm{Pa}}. \tag{2}$$

We also calculate the acoustic spectra at each Strouhal (St) number on an SPL basis via the relation

$$\mathrm{SPL_{St}} = 20\log_{10}\frac{S^{1/2}(X,\omega)}{2\times10^{-5}\ \mathrm{Pa}} + 10\log_{10}\frac{U_\infty}{\delta}, \tag{3}$$

where U_∞ denotes free-stream velocity in the stream-wise direction and δ is the boundary layer thickness.

Results

Aerodynamics

Numerical solutions are computed using the open-source SU2 solver [17]. We study free-stream subsonic Mach numbers of 0.30, 0.50, and 0.70 for the zero pressure gradient flat plate and the flat plate with a single suction port. Convergence of the solution is examined via the root mean square (RMS) value of residuals of ρ, ρU, ρV, ρE, k, and ω. A minimum residual value of 10^{-14} is sought, which enforces the solver iterations to stop if the residuals reach this value. Figure 2 shows the residual plots obtained for $M_\infty = 0.30$ for the flat plate and flat plate with suction port, respectively. The vertical axis is base ten log. We find the residuals approach a stable value towards the end of the iterations in both cases, from 0 to −6 for the different residual values in the case of Fig. 1 and roughly 0 to −5 for Fig. 2, which signal satisfactory convergence. The residual of the dissipation rate, ω, does not converge to the same order due to the numerically stiff equations and boundary conditions that result from the suction port. Residual of ω approaches a value of 2 to 4 in all CFD cases, regardless of M_∞. This is hypothesised being due to the computational domain near the suction port, which contains high aspect ratio cells to save computational expense.

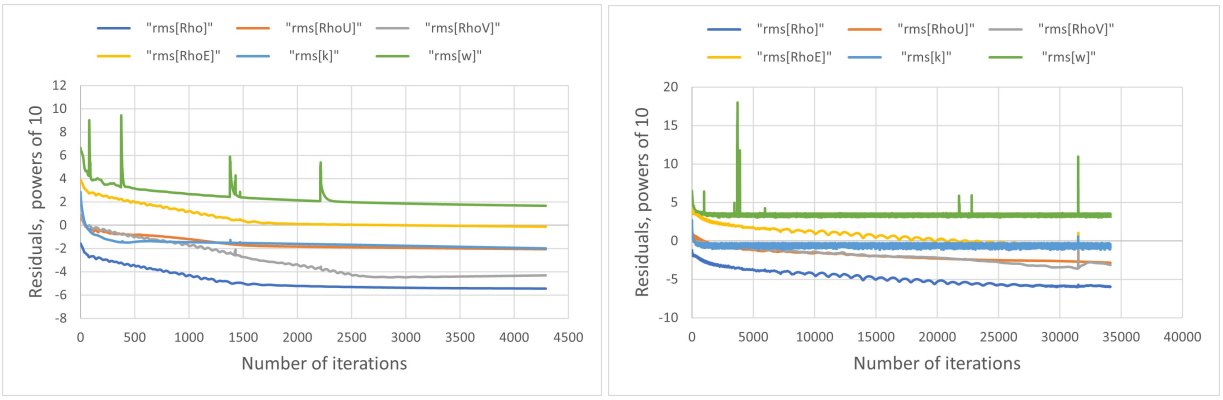

Fig. 2 Residual history for $M_\infty = 0.30$ for (a) flat plate and (b) flat plate with suction port.

Generally, convergence with suction ports takes significantly longer than cases without suction, irrespective of the value of M_∞. For example, for the convergence history shown in Fig. 2, convergence is achieved without a suction port at 4000 iterations. The same case with a suction port takes approximately 32000 iterations to converge. We verify whether or not the boundary layer is fully resolved within our mesh by comparing our flat plate mesh with the benchmark mesh from the NASA Turbulence Modeling Resource [18]. We accomplish this by plotting the composite boundary layer profile for both meshes for the same flow conditions, which is for the free-stream $M_\infty = 0.30$. This result is shown in Figure 3. The non-dimensionalized velocity, U^+, is plotted on the vertical axis against the non-dimensionalized

distance from the wall, Y^+, on the horizontal axis. The 'U+_actual' curve shown in Fig. 3 represents our prediction with SU2 and 'U+_tut' is the solution obtained with the mesh from NASA Langley. The vertical axis represents the non-dimensional velocity U^+, and the horizontal axis denotes the non-dimensional distance from the wall, Y^+. As shown in Fig. 3, the numerical results of the two cases show reasonable agreement until they both reach free-stream values of velocity. The predictions from SU2 using the computational domain from NASA approach a non-dimensional free-stream velocity of 20, whereas the mesh we created reaches a non-dimensional value of roughly 25. The error is observed to stem from the 'log-layer' of our mesh, which extends beyond that of the tutorial mesh.

We also show the static pressure contours in the region of the suction port for the three M_∞ cases investigated (0.30, 0.50, and 0.70) in Fig. 4. It is observed that as M_∞ increases, there is a pressure "hot spot" buildup at the right edge of the cavity (the pressure increases to 1.25 kPa from 1.15 kPa as M_∞ is increased from 0.30 to 0.70. This higher pressure region can be reduced by using a smaller suction port diameter, D, or reducing the pressure ratio from the free-stream to the suction port exit.

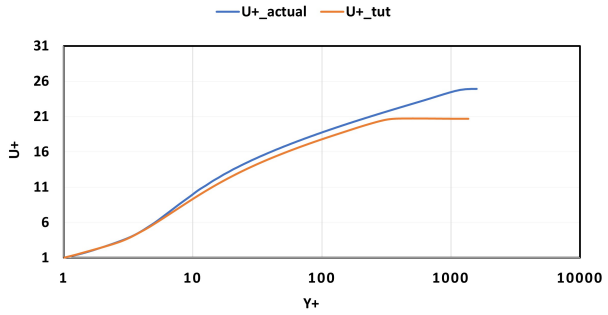

Fig. 3 Prediction compared to composite boundary layer profile at $M_\infty = 0.30$.

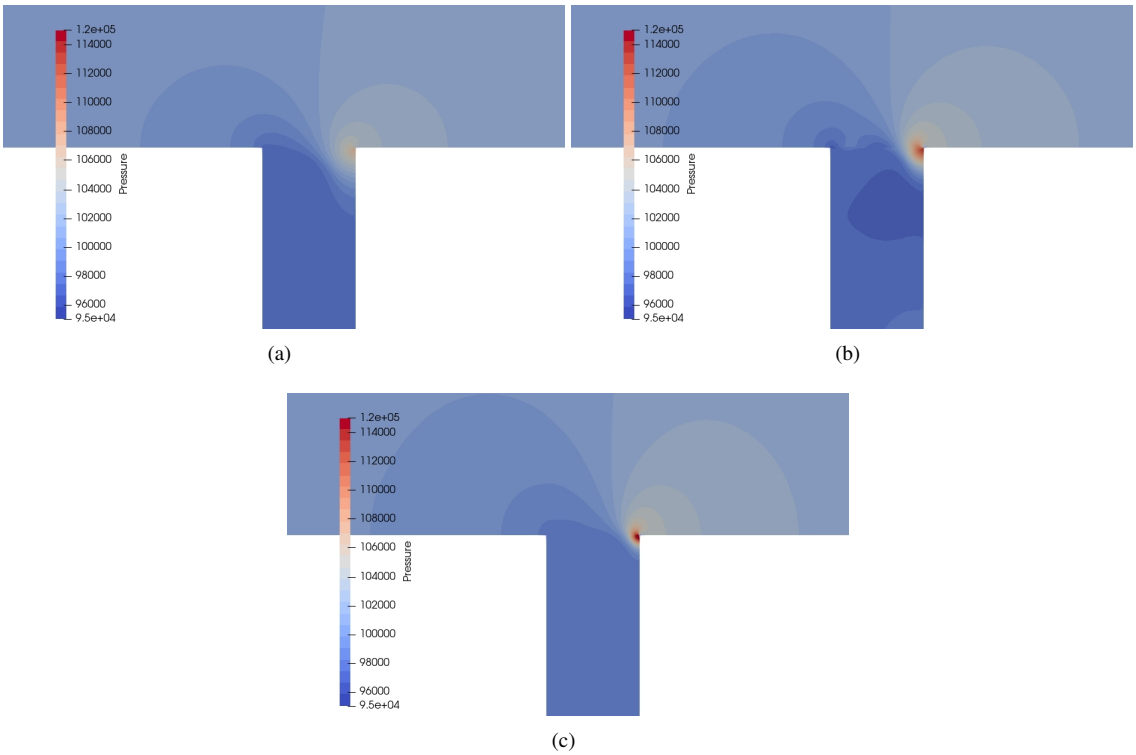

Fig. 4 Pressure contours near the suction port for (a) $M_\infty = 0.30$, (b) $M_\infty = 0.50$, and (c) $M_\infty = 0.70$.

Aeroacoustics

We evaluate Eqn. 1 to predict the acoustic spectra from the flat plate and the flat plate with the corresponding suction port for each Mach number. The noise is evaluated from the profile at x = 1.03 m, which is the distance on the plate from the leading edge and is also one port diameter from the suction port. We compare the change in sound pressure level (SPL) from the flat plate to the one with the suction port. ΔSPL denotes the difference of SPL relative to the case without suction to that with suction for each Mach number, i.e., $\Delta\text{SPL} = \text{SPL}_{\text{no suction}} - \text{SPL}_{\text{suction}}$. Therefore, a positive ΔSPL indicates a reduction of noise on a per frequency basis. Figure 5 shows the ΔSPL for each M_∞ with increasing frequency, f. It is observed that at $M_\infty = 0.30$, suction leads to increased noise compared to the case without suction. Here, ΔSPL being negative in the range of 10 Hz to 10 kHz indicates a large noise increase of approximately 10 dB. Beyond this frequency range, ΔSPL is observed to rise above zero, reaching a peak of 20.54 dB reduction at 79.43 kHz. At $M_\infty = 0.50$ and 0.70, suction is observed to lead to noise reduction at all frequencies, evidenced by the curve being above zero across all values of f. For $M_\infty = 0.50$, in the range of 10 Hz to 1000 Hz, we predict a 35 dB reduction in noise. Then, we observe a sharp reduction in the curve (which indicates more noise produced due to suction) until a frequency of approximately 10 kHz. The curve is observed to rise again at higher frequencies, which indicates that the suction reduces noise at those frequencies. We predict the rise to peak at 62.08 dB at the last measured data point of 158.49 kHz. For $M_\infty = 0.70$, we observe noise reduction of the order of 200 dB across all frequencies, which signifies that at this point in the flow the turbulence is not creating any significant noise.

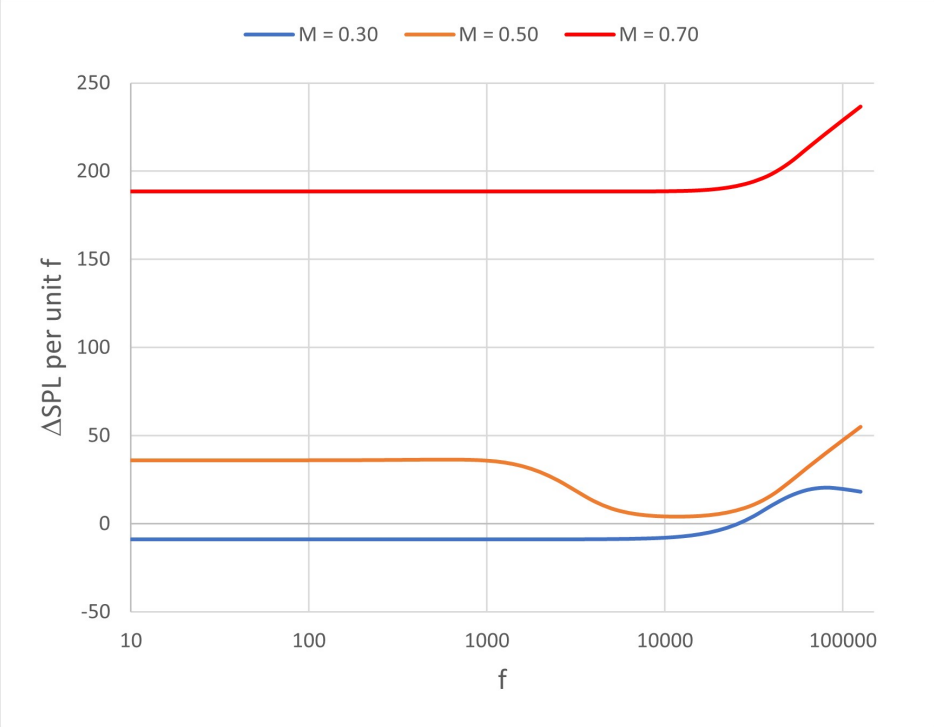

Fig. 5 Variation of ΔSPL with f for the three Mach number cases.

We show the variation of the source term, $S(X, \omega)$, calculated from Eqn. 1 across the boundary layer for particular values of f and free-stream M_∞. The frequency values are chosen to represent areas of significant changes in the acoustic spectra curve as it varies with f. For $M_\infty = 0.30$, Fig. 6 shows the source distribution for f of 10 Hz in Fig. 6(a) and 31 kHz in Fig. 6(b). Similarly, for $M_\infty = 0.50$, Fig. 7(a) shows the source distribution for f at 100 Hz and Fig. 7(b) shows the same at 10 kHz. The curve of $M_\infty = 0.70$ versus f is neglected as we observed in Fig. 5 that there is negligible acoustic radiation when suction is present for this case.

The vertical axis in both Figs. 6 and 7 denote the source $S(X, \omega)$ in Pa^2 per unit Hz. The horizontal axis represents increasing perpendicular distance from the wall in meters located at a point on the plate where the flow profile is extracted, i.e., x = 1.03 m. It is observed that in Fig. 6(a), the source term of noise in the presence of suction, denoted by 'S_suction' dominates over the source term of noise when suction is not present, represented here by 'S_base.' This

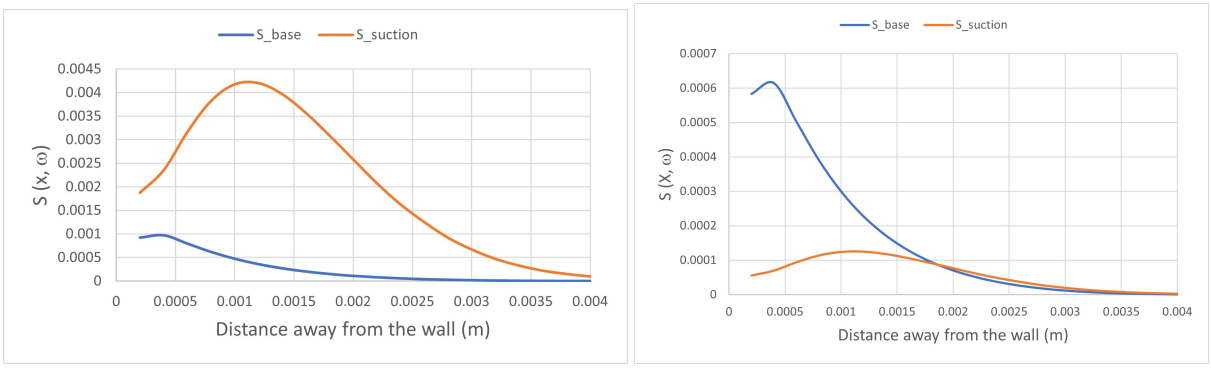

(a) (b)

Fig. 6 Noise source distribution away from the wall for $M_\infty = 0.30$ at (a) 10 Hz and (b) 31 kHz.

is in alignment with what we see in Fig. 5 at 10 Hz for $M_\infty = 0.30$ and shows how suction leads to increased noise at lower subsonic Mach numbers. Figure 6(b) shows a similar source distribution at 31 kHz for the same free-stream Mach number. Contrary to what is observed in Fig. 6(a) and in agreement with Fig. 5 of the ΔSPL versus f and M_∞ value, we observe that 'S_base' dominates over 'S_suction' across most of y. This yields a rise in acoustic radiation as seen in extremities of the $M_\infty = 0.30$ curve in Fig. 5.

We show similar source distribution curves for $M_\infty = 0.50$ at frequencies of 100 Hz and 10 kHz. These values are chosen to represent source distributions at points of the curve in Fig. 5 experiencing different ΔSPL values. For instance, at 100 Hz, there is a decrease of 35.98 dB due to suction and at 10 kHz, this value reduces to 4.23 dB. Figures 7(a) and 7(b) show these source distributions, denoted by 'S_suction' and 'S_base,' with increasing distance away from the wall at 100 Hz and 10 kHz, respectively. The fact that at 100 Hz, we obtain a higher noise reduction than at 10 kHz (35.98 dB against 4.23 dB) is reflected in the corresponding source distribution curves. We can clearly see a dominance of the 'S_base' term in Fig. 7(a) that is not seen in Fig. 7(b), which is observed in corresponding ΔSPL values. How the turbulent kinetic energy (TKE) develops over the boundary layer and beyond for both the suction and

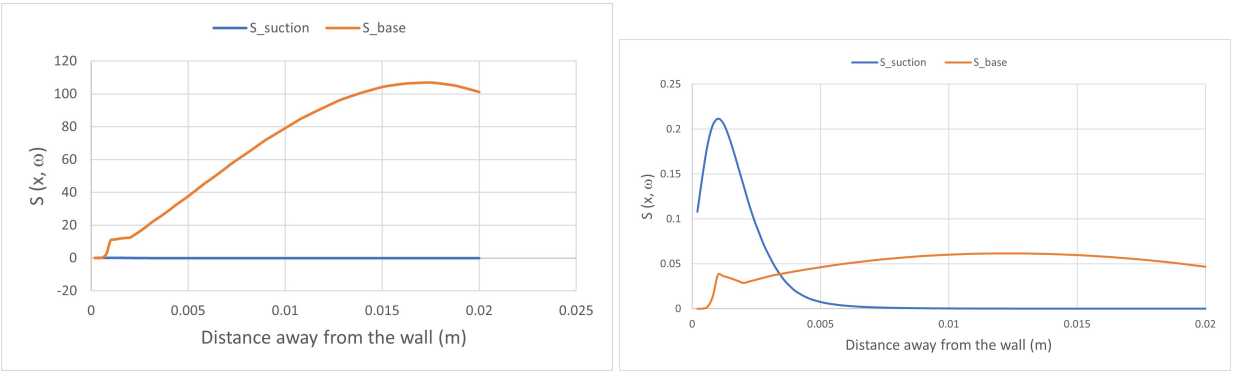

(a) (b)

Fig. 7 Noise source distribution away from the wall for $M_\infty = 0.50$ at (a) 100 Hz and (b) 10 kHz.

base case is investigated as this provides insight into how the turbulence is altered by suction. Figure 8 shows how TKE develops for the three M_∞ investigated. The vertical axis represents TKE in m^2/s^2 and the horizontal axis denotes the increasing cross-stream distance from the wall at $x = 1.03$ m (one port diameter distance upstream from the suction port). Comparing ΔSPL curves shown earlier in Fig. 5, it is observed that the variation in TKE with or without suction does not have a direct correlation with the observed ΔSPL values. For example, when suction leads to a decrease in noise generated, it does not necessarily mean that the TKE curve when suction is present falls under the TKE curve when suction is not present. An example of this is shown in Fig. 8(c), where variation in TKE at $M_\infty = 0.70$ is shown for when suction is present and when it is not. Here, suction leads to a drastic reduction in noise as evidenced in Fig.

5. However in Fig. 8(c), we observe that in some ranges (0 to 0.004 m), the curve of TKE, when suction is present ('TKE_Suction') looms over the curve of TKE when suction is absent ('TKE_Base').

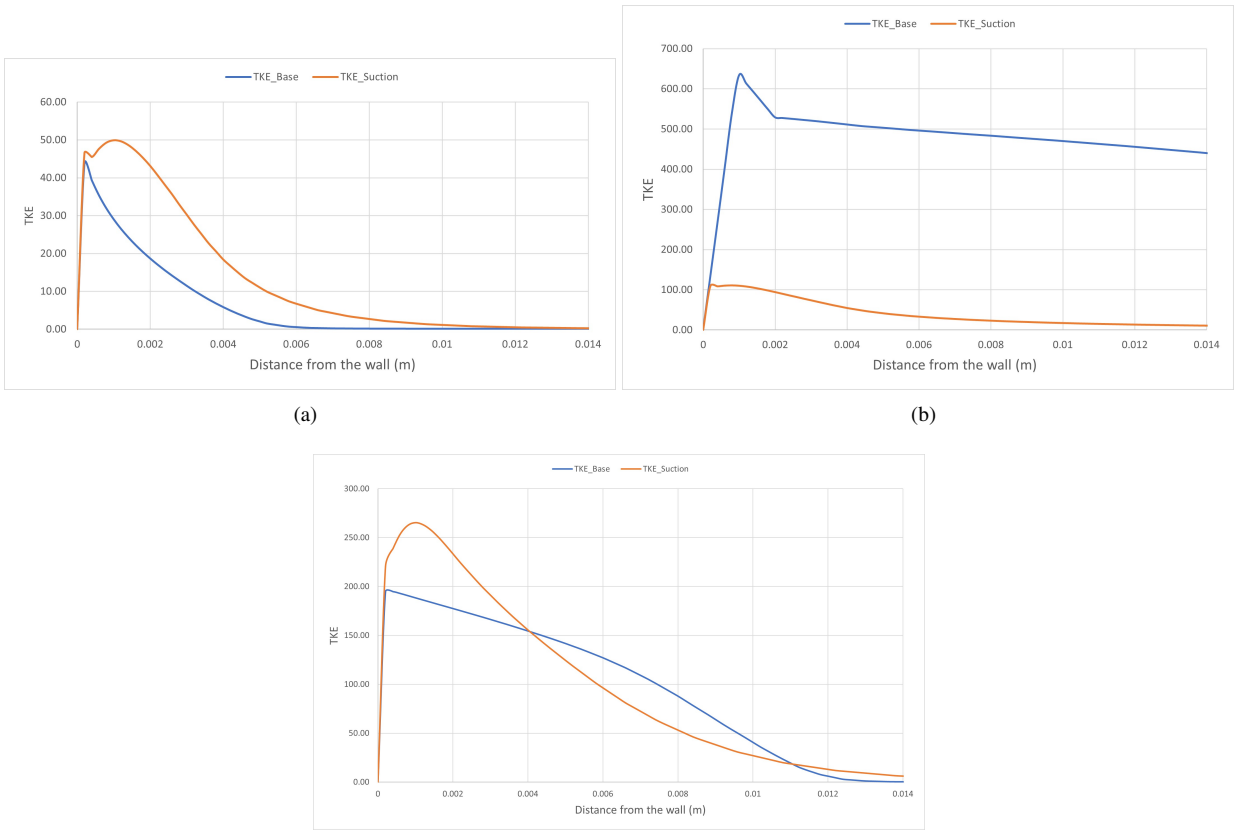

Fig. 8 Turbulent kinetic energy (TKE) variation with distance away from the wall for (a) $M_\infty = 0.30$**, (b)** $M_\infty = 0.50$**, and (c)** $M_\infty = 0.70$

.

I. Summary and Conclusion

To summarize, we examined the acoustic radiation arising from zero pressure gradient turbulent boundary layers with and without the presence of suction at three subsonic Mach numbers for a constant static pressure suction outlet employing the CSAA of Miller [11]. We predicted the change in SPL when suction is present relative to a base case across varying frequencies for the turbulent statistics extracted from the flow solution at one port distance from the suction port ($x = 1.03$ m from the leading edge). The suction port is located 0.99 m from the leading edge and spans 0.02 m across. We showed the source distributions across the boundary layer at certain frequencies for $M_\infty = 0.30$ and 0.50. We also determined the change in turbulent kinetic energy (TKE) across the boundary layer for all the flows and observed the relation between change in TKE and the noise radiated with suction. We observed that suction leads to higher noise at lower Mach numbers and reduced acoustic radiation at higher subsonic Mach numbers for the domain studied. At the highest Mach number studied, we observed elimination of noise from the turbulence due to the suction port. This is not to say that there is no noise from the flow at $M_\infty = 0.70$, as significant pressure loading on the plate will occur that represents another noise source. We also observed that there is no direct correlation between TKE and the change in SPL observed.

In the future, we propose to examine the noise from flows with more complicated suction geometries and the effect of multiple ports. This way, the results can be generalized to more realistic geometries. In this study, we used a constant pressure suction outlet. How the noise prediction varies with varying back pressure of the suction port should also be

examined.

References

[1] Prandtl, L., "On Fluid Motion with Very Small Friction," *Heidelberg Mathematical Congress*, 1904.

[2] Schlichting, H., and Gersten, K., *Boundary-Layer Theory*, Springer Berlin Heidelberg, 2017. https://doi.org/10.1007/978-3-662-52919-5, URL https://doi.org/10.1007/978-3-662-52919-5.

[3] Oyewola, O., Djenidi, L., and Antonia, R. A., "Combined influence of the Reynolds number and localised wall suction on a turbulent boundary layer," *Experiments in Fluids*, Vol. 35, No. 2, 2003, pp. 199–206. https://doi.org/10.1007/s00348-003-0658-1, URL https://doi.org/10.1007/s00348-003-0658-1.

[4] Zhu, Y., and Antonia, R. A., "Effect of concentrated wall suction on the structure of a turbulent boundary layer," *Proceedings of 12th Australasian Fluid Mechanics Conference*, 1995, pp. 215–218.

[5] Djenidi, L., Gall, P.-E., Vincent, A., and Antonia, R., "Effect of Wall Suction on the Structure of a Turbulent Boundary Layer," *14th Australasian Fluid Mechanics Conference Adelaide University, Adelaide, Australia*, 2002.

[6] Reynolds, G. A., and Saric, W. S., "Experiments on the stability of the flat-plate boundary layer with suction," *AIAA Journal*, Vol. 24, No. 2, 1986, pp. 202–207. https://doi.org/10.2514/3.9246, URL https://doi.org/10.2514/3.9246.

[7] Antonia, R. A., Spalart, P. R., and Mariani, P., "Effect of suction on the near-wall anisotropy of a turbulent boundary layer," *Physics of Fluids*, Vol. 6, No. 1, 1994, pp. 430–432. https://doi.org/10.1063/1.868043, URL https://doi.org/10.1063/1.868043.

[8] Park, J., and Choi, H., "Effects of uniform blowing or suction from a spanwise slot on a turbulent boundary layer flow," *Physics of Fluids*, Vol. 11, No. 10, 1999, pp. 3095–3105. https://doi.org/10.1063/1.870167, URL https://doi.org/10.1063/1.870167.

[9] Kametani, Y., Fukagata, K., Örlü, R., and Schlatter, P., "Effect of uniform blowing/suction in a turbulent boundary layer at moderate Reynolds number," *International Journal of Heat and Fluid Flow*, Vol. 55, 2015, pp. 132–142. https://doi.org/10.1016/j.ijheatfluidflow.2015.05.019, URL https://doi.org/10.1016/j.ijheatfluidflow.2015.05.019.

[10] Bobke, A., Örlü, R., and Schlatter, P., "Simulations of turbulent asymptotic suction boundary layers," *Journal of Turbulence*, Vol. 17, No. 2, 2015, pp. 157–180. https://doi.org/10.1080/14685248.2015.1083574, URL https://doi.org/10.1080/14685248.2015.1083574.

[11] Miller, S. A. E., "Prediction of Turbulent Boundary-Layer Noise," *AIAA Journal*, Vol. 55, No. 5, 2017, pp. 1659–1672. https://doi.org/10.2514/1.j055087, URL https://doi.org/10.2514/1.j055087.

[12] Menter, F. R., "Two-equation eddy-viscosity turbulence models for engineering applications," *AIAA Journal*, Vol. 32, No. 8, 1994, pp. 1598–1605. https://doi.org/10.2514/3.12149, URL https://doi.org/10.2514/3.12149.

[13] Geuzaine, C., and Remacle, J.-F., "Gmsh: A 3-D finite element mesh generator with built-in pre- and post-processing facilities," *International Journal for Numerical Methods in Engineering*, Vol. 79, No. 11, 2009, pp. 1309–1331. https://doi.org/10.1002/nme.2579, URL https://doi.org/10.1002/nme.2579.

[14] Lighthill, M. J., "On sound generated aerodynamically I. General theory," *Proceedings of the Royal Society of London. Series A. Mathematical and Physical Sciences*, Vol. 211, No. 1107, 1952, pp. 564–587. https://doi.org/10.1098/rspa.1952.0060, URL https://doi.org/10.1098/rspa.1952.0060.

[15] Efimtsov, B., "Characteristics of the field of turbulent wall pressure-fluctuations at large Reynolds-numbers," *Soviet Physics Acoustics-USSR*, Vol. 28, No. 4, 1982, pp. 289–292.

[16] Powell, A., "Aerodynamic Noise and the Plane Boundary," *The Journal of the Acoustical Society of America*, Vol. 32, No. 8, 1960, pp. 982–990. https://doi.org/10.1121/1.1908347, URL https://doi.org/10.1121/1.1908347.

[17] Palacios, F., Alonso, J., Duraisamy, K., Colonno, M., Hicken, J., Aranake, A., Campos, A., Copeland, S., Economon, T., Lonkar, A., Lukaczyk, T., and Taylor, T., "Stanford University Unstructured (SU): An open-source integrated computational environment for multi-physics simulation and design," *51st AIAA Aerospace Sciences Meeting including the New Horizons Forum and Aerospace Exposition*, American Institute of Aeronautics and Astronautics, 2013. https://doi.org/10.2514/6.2013-287, URL https://doi.org/10.2514/6.2013-287.

[18] Christopher, R., "2D Zero Pressure Gradient Flat Plate Validation Case," *NASA Langley Research Center*, 2020. URL https://turbmodels.larc.nasa.gov/flatplate_val.html.